6206 *Biochemistry* **2010,** *49,* 6206–6218
DOI: 10.1021/bi100728q

BIOCHEMISTRY
including biophysical chemistry & molecular biology
Article

Structural Basis for Hydration Dynamics in Radical Stabilization of Bilin Reductase Mutants[†,‡]

Amanda C. Kohler,[§,▽] David D. Gae,[⊥] Michael A. Richley,[∥] Stefan Stoll,[§] Alexander Gunn,[§] Sunghyuk Lim,[§] Shelley S. Martin,[∥] Tzanko I. Doukov,[#] R. David Britt,[§] James B. Ames,[§] J. Clark Lagarias,[∥] and Andrew J. Fisher*[,§,∥]

[§]*Department of Chemistry,* [∥]*Department of Molecular and Cellular Biology, and* [⊥]*Biophysics Graduate Program, University of California, One Shields Avenue, Davis, California 95616, and* [#]*Stanford Synchrotron Radiation Lightsource, Menlo Park, California 94025* [▽]*Current Address: Laboratory of Structural Microbiology, Rockefeller University, New York, NY 10065*

Received May 7, 2010; Revised Manuscript Received June 16, 2010

ABSTRACT: Heme-derived linear tetrapyrroles (phytobilins) in phycobiliproteins and phytochromes perform critical light-harvesting and light-sensing roles in oxygenic photosynthetic organisms. A key enzyme in their biogenesis, phycocyanobilin:ferredoxin oxidoreductase (PcyA), catalyzes the overall four-electron reduction of biliverdin IXα to phycocyanobilin—the common chromophore precursor for both classes of biliproteins. This interconversion occurs via semireduced bilin radical intermediates that are profoundly stabilized by selected mutations of two critical catalytic residues, Asp105 and His88. To understand the structural basis for this stabilization and to gain insight into the overall catalytic mechanism, we report the high-resolution crystal structures of substrate-loaded Asp105Asn and His88Gln mutants of *Synechocystis* sp. PCC 6803 PcyA in the initial oxidized and one-electron reduced radical states. Unlike wild-type PcyA, both mutants possess a bilin-interacting axial water molecule that is ejected from the active site upon formation of the enzyme-bound neutral radical complex. Structural studies of both mutants also show that the side chain of Glu76 is unfavorably located for D-ring vinyl reduction. On the basis of these structures and companion $^{15}N-^{1}H$ long-range HMQC NMR analyses to assess the protonation state of histidine residues, we propose a new mechanistic scheme for PcyA-mediated reduction of both vinyl groups of biliverdin wherein an axial water molecule, which prematurely binds and ejects from both mutants upon one electron reduction, is required for catalytic turnover of the semireduced state.

Linear tetrapyrroles (bilins) perform important roles in the biology of bacteria, algae, plants, and animals. Bilins (aka. bile pigments) were first identified in animals, where they are formed during metabolic breakdown of heme to recycle iron (*1*, *2*). In photosynthetic organisms, bilins covalently associated with proteins to carry out light-sensing functions vital to optimizing photosynthesis and light capture (*3*, *4*). As prosthetic groups of phytochromes, photoreceptors widely distributed in photosynthetic and some nonphotosynthetic organisms, bilins are activated by light to regulate complex signaling cascades during photomorphogenesis (*5*). The bilin prosthetic groups of phycobiliproteins of cyanobacteria, red algae, and cryptomonads also function as light harvesting antennae to efficiently transfer light energy to photosynthetic reaction centers (*6*). [1]

Bilins in nature are primarily generated from the enzyme-mediated degradation of heme. The oxygen-dependent interconversion of heme to biliverdin IXα (BV), catalyzed by the enzyme heme oxygenase, occurs widely among obligate aerobic and facultative anaerobic organisms (*4*, *7*−*9*). Strongly product-inhibited, heme oxygenase turnover is facilitated by BV reduction or removal by binding to bilin-binding proteins. In animals, BV is converted to bilirubin IXα by the NAD(P)H-dependent enzyme biliverdin reductase (*10*, *11*). By contrast, in oxygenic photosynthetic organisms, BV is reduced by ferredoxin-dependent bilin reductases (FDBRs) to produce the phytobilins: phytochromobilin (PΦB), phycocyanobilin (PCB), and phycoerythrobilin (PEB) (*3*, *4*).

Originally identified in oxygenic photosynthetic organisms, FDBRs have been classified into five subfamilies that correspond to their unique substrate and/or product specificities (*12*). Owing to the recent discovery of PEB synthase (PebS), an FDBR encoded by a marine cyanophage, (*13*) and to the existence of novel bilins in cryptomonads whose biosynthesis is not yet understood (*14*), novel members of the FDBR family are expected to be discovered in photosynthetic organisms whose genomes have yet to be characterized. The best characterized FDBR is phycocyanobilin:ferredoxin oxidoreductase (PcyA, EC 1.3.7.5), which catalyzes the four-electron reduction of BV to PCB (Figure 1A, (*15*)). Like all known members of the FDBR family, PcyA possesses neither metal nor organic cofactors to mediate sequential one-electron, ferredoxin-mediated reduction of its bilin substrate. It was therefore hypothesized, and later shown for PcyA, that BV reduction proceeds through bilin radical intermediates that are regiospecifically protonated to yield its phytobilin product PCB (*16*). Using chemical modification, site-specific

[†]This work was supported in part by National Science Foundation grant MCB-0843625 to A.J.F. and J.C.L., and by NIH grant GM73789 to R.D.B. and EY012347 to J.B.A. A National Institutes of Health training grant T32-GM007377 supported D.D.G.

[‡]Protein coordinates have been deposited in the Protein Data Bank (IDs 3nb8, 3nb9, 3f0l, and 3f0m for the H88Q oxidized, H88Q radical, D105N oxidized, and D105N radical complexes, respectively).

*To whom correspondence should be addressed. E-mail: fisher@chem.ucdavis.edu. Phone: 530-754-6180. Fax: 530-752-8995.

[1]Abbreviations: FDBR, ferredoxin-dependent bilin reductase; PCB, phycocyanobilin; BV, biliverdin IXα; BV13, biliverdin 13; DHBV, 18^{1},18^{2}-dihydrobiliverdin IXα; THBV, tetrahydrobiliverdin IXα; Fd, ferredoxin; FNR, ferredoxin:NADP oxidoreductase; PcyA, phycocyanobilin:ferredoxin oxidoreductase; rmsd, root-mean-square deviation.

 Published on Web 06/17/2010

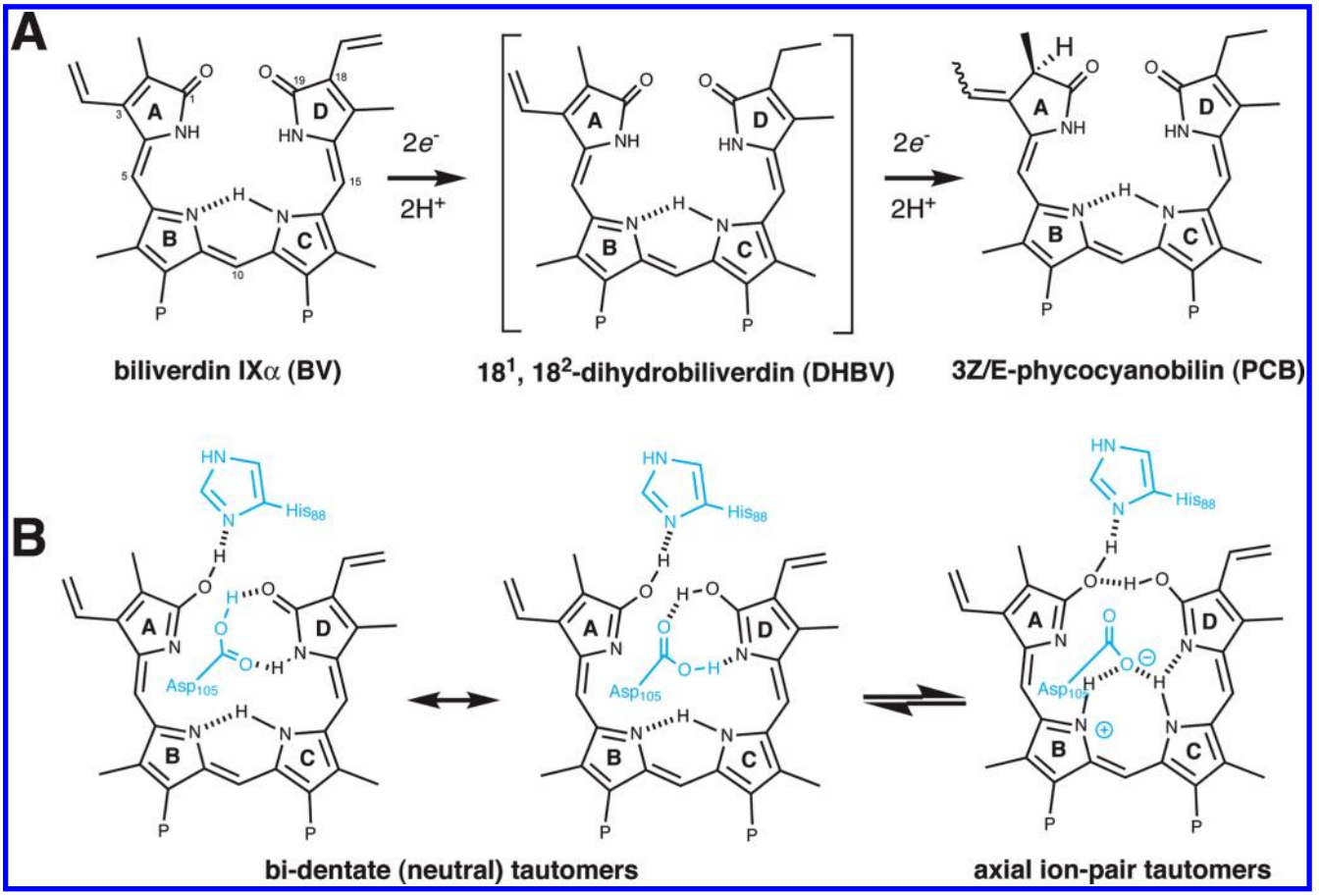

FIGURE 1: PcyA reaction. (A) PcyA catalyzes the four-electron reduction of biliverdin (BV) to phycocyanobilin (PCB) via the intermediacy of 18^1,18^2-dihydrobiliverdin (*15*). Four proton-coupled-electron-transfers are mediated by stepwise one-electron transfers from four reduced ferredoxins (Fd). Pyrrole rings are labeled A−D, "P" represents the propionate groups, and the small numbers indicate carbon numbering for BV. (B) Different tautomeric forms of Asp105 with the D-ring pyrrole for wild-type PcyA. The major "bidentate" neutral conformation observed as 65% occupancy (*19*) is depicted both neutral lactam and lactim tautomers. The minor "axial" ion-pair conformation is shown on the right. Dashed lines represent hydrogen bonds. The positive charge of the minor conformation on the B-ring also can be delocalized on other pyrrole rings and on His88.

mutagenesis, and substrate analogue experiments, a mechanism for the PcyA-mediated conversion of BV to PCB via the two-electron reduced intermediate 18^1,18^2-dihydrobiliverdin (DHBV) was subsequently proposed (*17*, *18*).

High-resolution structures of PcyA from the cyanobacteria *Synechocystis* sp. PCC6803 (*19*−*21*) and *Nostoc* sp. PCC7120 (*18*) reveal a central seven-stranded antiparallel β-sheet that is sandwiched on either side by four α-helixes. The substrate-bound PcyA structure shows that BV inserts between the β-sheet and helices seven and eight (*19*). In substrate-free PcyA, the His88 imidazolium side chain forms a clear salt linkage with the carboxylate side chain of Asp105 (*Synechocystis* numbering), a linkage that is disrupted to accommodate BV binding. The catalytic importance of these residues is underscored by the observation that mutation of either His88 or Asp105 drastically inhibits catalytic turnover (*17*). Interestingly, both H88Q and D105N mutants of PcyA generate stable, catalytically stalled bilin radical complexes that fail to be further reduced in the presence of excess reductant (*17*). The unusual stabilization of bilin radical intermediates indicates that both residues play critical roles in subsequent proton-coupled electron transfers mediated by PcyA.

The present work was undertaken to determine the structural basis of the stability of the semireduced BV radical intermediates in the H88Q and D105N mutants and their inability to support full catalytic turnover. Owing to the large size of ferredoxin, our studies exploit the small chemical reductant sodium dithionite to generate the trapped bilin radical intermediates in situ for both mutants in the crystalline state (*22*). Here we report the 1.3−1.5 Å resolution crystal structures of the BV-substrate loaded H88Q and D105N mutants of PcyA before and after reduction with sodium dithionite. Companion studies also address the protonation state of histidine residues using $^{15}N-^{1}H$ HMQC NMR spectroscopy. In addition to shedding new insight into the structural basis of bilin reduction, these investigations provide compelling support for the importance of both residues and a water molecule that becomes associated with the bilin substrate during catalysis in proton-coupled electron transfer by PcyA.

EXPERIMENTAL PROCEDURES

Site-Directed Mutagenesis, Expression, and Purification of Synechocystis PcyA. Site-directed mutagenesis of *Synechocystis* PcyA cloned in the pTYB12 vector (New England BioLabs, Ipswich, MA) was performed using the QuikChange XL site-directed mutagenesis kit (Stratagene, La Jolla, CA). D105N and H88Q mutant clones, confirmed by DNA sequencing (Davis Sequencing, Davis, CA), were transformed into *Escherichia coli* strain BL21-DE3 (Stratagene, La Jolla, CA) for protein expression. After lactose induction at 12 °C for 19 h, mutant proteins were purified according to the IMPACT-CN protein purification protocol (New England BioLabs, Beverly,

MA) with the following modifications. Cell lysis buffer consisted of 50 mM Tris-HCl, pH 8.0, 0.5 M NaCl, and 0.1% v/v Triton-X 100, and the column equilibration buffer consisted of 50 mM Tris, pH 8.0, 0.5 M NaCl. On-column cleavage was performed by addition of 50 mM 2-mercaptoethanol to column equilibration buffer (50 mM Tris-HCl, pH 8.0, 0.5 M NaCl) followed by incubation at 4 °C for 48 h. Purified protein was dialyzed in 20 mM Tris-HCl, pH 8.0 for 24 h followed by concentration using Amicon Ultra 10,000 MWCO centrifugal tubes (Millipore Corp, Billerica, MA) to approximately 10 mg/mL. Concentrated PcyA protein was stored at −80 °C prior to use.

Crystallization of Synechocystis PcyA Mutants. Crystallization of BV substrate-loaded PcyA was performed under green safelight using the hanging-drop method with a drop size of 4 μL on 24-well Linbro plates using BV-loaded PcyA D105N and H88Q mutants. BV loading was performed by adding a stoichiometric amount of BV to the enzyme 30 min prior to crystal setup. Crystallization drops contained 2 μL of reservoir buffer plus 2 μL of 10 mg/mL PcyA:BV solution, which were suspended over reservoir buffer. Crystals were grown at 293 K in the dark. Conditions that resulted in the best diffracting dithionite-treated "reduced" D105N PcyA crystals were 1.45−1.8 M ammonium sulfate, 0.15−0.4 M NaCl, and 0.1 M HEPES pH 7.0. Conditions that resulted in the best diffracting dithionite-treated "reduced" H88Q PcyA crystals were 1.7−2.2 M ammonium sulfate, 0.26−0.32 M NaCl, and 0.1 M sodium cacodylate pH 7.0. These conditions produced long, rectangular crystals that were dark blue in their native state.

Diffraction Data Collection of Synechocystis PcyA. Individual PcyA crystals were sequentially transferred into a cryoprotectant solution consisting of 30% (v/v) ethylene glycol in mother liquor and flash frozen in liquid nitrogen. For in situ reduction, substrate-bound H88Q and D105N PcyA crystals were soaked with 100 mM sodium dithionite in reservoir buffer solutions and allowed to sit in the dark until a color change from blue to green occurred, typically within 10 min. X-ray diffraction data from untreated "oxidized" and dithionite-treated "reduced" BV substrate-bound H88Q and D105N PcyA crystals were collected on beamline 7−1 at the Stanford Synchrotron Radiation Lightsource (SSRL). Diffraction data were indexed and integrated using Mosflm and scaled with the CCP4 program SCALA. Oxidized H88Q and D105N data sets were resolved to 1.3 Å resolution with a completeness of 90.1% and 97.6%, respectively. Both mutants crystallized in space group $P2_12_12$ with unit cell parameters of: a = 70.8 Å, b = 95.6 Å, c = 42.7 Å. Oxidized H88Q and D105N crystals had a calculated Matthews coefficient V_M (*23*) of 2.3 Å^3/Da (~45% solvent content) and 2.1 Å^3/Da (~42% solvent content), respectively, assuming one monomer per crystallographic asymmetric unit (ASU).

Synchrotron X-ray radiation has been shown to reduce cofactors in enzymes (*24*−*26*). To monitor the potential reduction of the radical intermediate, microspectrometry was used to record changes in the UV/vis spectrum of the crystal during exposure to the X-ray beam. Spectral changes in the visible spectrum correlates well with reduction state of BV bound to PcyA in solution (*16*). To limit the reduction potential from X-ray radiation, our radical structure data sets resulted from the merging of diffraction data collected in 12° increments from five reduced H88Q crystals and 10 reduced D105N crystals. Each 12° increment had less than 60 s of X-ray radiation exposure (or radiation dose of 0.064 MGy). Reduced H88Q and D105N data sets were resolved to 1.5 Å resolution with a completeness of 80.6% and 95.2%, respectively. Diffraction data on the initial oxidized mutants were collected from a single crystal of each mutant. The oxidized crystals were exposed in the X-ray beam for a total time of 8 min (radiation dose of 0.51 MGy) to collect a complete data set. The X-ray radiation dose absorbed by crystals was calculated using the program RADDOSE (*27*).

Mutant Synechocystis PcyA Structure Determination, Model Building, and Structure Refinement. Structures were solved by molecular replacement using the wild-type *Synechocystis* PcyA structure (PDB ID: 2d1e) (*19*). Model building was performed using the molecular graphics program COOT (*28*). Maximum-likelihood coordinate and *B*-factor refinement was carried out with the program REFMAC (*29*) using 95% of the collected data to the respective maximum resolution (5% of the data was set aside for R_{free} cross validation). Model quality was checked using the program PROCHECK (*30*), and the results are summarized in Table 1.

EPR Spectroscopy. EPR spectroscopy was performed at the CalEPR facility using a laboratory-constructed pulsed EPR spectrometer operating at 130 GHz (D-band) with the oscillating magnetic field of the cylindrical microwave resonator perpendicular to the applied magnetic field. The D-band spectrometer was described previously in a 130 GHz EPR spectroscopic characterization of the D105N mutant of PcyA (*22*). A single crystal of the H88Q mutant of PcyA was soaked in sodium dithionite solution and mounted inside of a 0.5 mm ID quartz capillary with the long crystal axis parallel to the capillary axis and flash frozen in liquid nitrogen.

NMR Spectroscopy. ^{15}N-labeled PcyA samples, obtained from cells grown on ^{15}N-$(NH_4)_2SO_4$ supplemented minimal media (*31*), were buffer-exchanged into 95% H_2O/5% D_2O solution containing 10 mM phosphate (pH 7.0) to a final protein concentration of ~0.5 mM. All NMR experiments were performed at 25 °C on a Bruker Avance III 600 MHz spectrometer equipped with a four-channel interface and triple-resonance cryoprobe (TCI) with pulsed field gradients. Two-dimensional ^{15}N−^{1}H long-range HMQC (LR-HMQC) NMR experiments were performed to correlate histidine ring nitrogen-15 resonances ($N_{\delta 1}$ and $N_{\varepsilon 2}$) with carbon-attached ring protons, $H_{\delta 2}$ and $H_{\varepsilon 1}$. A dephasing delay of 45 ms was chosen to select the desired two-bond correlations ($^2J_{NH}$ = 11.35 Hz) in the histidine ring and to suppress signals from one-bond $^1J_{NH}$ amide couplings (*32*). LR-HMQC spectra of uniformly ^{15}N-labeled PcyA and mutants (H88Q and D105N) were performed with ^{1}H and ^{15}N carrier frequencies at 4.70 and 210 ppm, respectively. The ^{15}N dimension had a sweep width of 110 ppm with 128 complex points, and the ^{1}H dimension had a sweep width of 12 ppm with 2048 complex points. Decoupling of ^{15}N was accomplished with the GARP sequence (*33*) using a 1.39 kHz field.

RESULTS

Both PcyA Mutants Contain a Tightly Bound Water Molecule in Their Active Sites, Not Seen in Wild-Type. Crystal structures were determined for the PcyA mutants D105N and H88Q with bound BV at 1.3 Å resolution, which represents the initial "oxidized" substrate-bound Michaelis complex. Of the possible 248 amino acids, electron density clearly defines residues 6−248 and 5−247 for D105N and H88Q mutants, respectively. Both D105N and H88Q mutants adopt α/β/α sandwich folds possessing a central seven-stranded antiparallel β-sheet lying between four α-helixes on each side (Figure 2A). Other than

Table 1: Data Collection, Phasing, and Refinement Statistics

	H88Q PcyA w/BV oxidized	H88Q PcyA w/BV radical	D105N PcyA w/BV oxidized	D105N PcyA w/BV radical
Data Collection Statistics				
X-ray source	SSRL BL7−1	SSRL BL7−1	SSRL BL7−1	SSRL BL7−1
wavelength (Å)	0.978	0.978	0.978	0.978
no. of crystals	1	5	1	10
radiation dose/crystal (MGy)	0.51	0.064	0.51	0.064
resolution (Å)	1.30 (1.33−1.30)	1.50 (1.54−1.50)	1.30 (1.33−1.30)	1.50 (1.54−1.50)
space group	$P2_12_12$	$P2_12_12$	$P2_12_12$	$P2_12_12$
cell parameters (Å)	a = 70.8	a = 70.8	a = 70.8	a = 70.9
	b = 95.6	b = 95.2	b = 95.6	b = 95.2
	c = 42.7	c = 42.6	c = 42.7	c = 42.5
monomers/ASU	1	1	1	1
V_M (Å^3/Da); % solvent (%)	2.3; 45.1	2.2; 44.6	2.3; 45.1	2.2; 43.0
no. of reflections	281087	75009	286749	120914
no. unique reflections	64782	37241	69979	44652
R_{merge}[a] (%)	4.2 (19.4)	7.9 (18.8)	5.2 (20.7)	7.8 (31.8)
mean (I)/σ(I)	20.0 (3.8)	9.3 (3.3)	14.4 (2.0)	10.8 (2.9)
completeness (%)	90.1 (79.2)	80.6 (74.0)	97.6 (95.4)	95.2 (88.7)
Refinement Statistics				
resolution (Å)	26.21−1.30	27.23−1.50	39.62−1.30	42.56−1.50
no. of reflections ($F \geq 0$)	61469 (3967)	35380 (2317)	66484 (4783)	43061 (2896)
R-factor[b] (%)	16.8 (22.8)	17.1 (24.3)	16.9 (26.0)	17.4 (23.9)
R-free[b] (%)	19.1 (24.2)	19.6 (24.5)	19.3 (23.8)	21.2 (28.9)
rms bond lengths (Å)	0.017	0.019	0.015	0.019
rms bond angles (deg)	2.043	2.124	1.721	1.943
estimated coordinate error (ESU based on R-free value) (Å)	0.053	0.083	0.049	0.077
overall mean B values (Å^2)	16.22	16.18	16.12	17.82
Ramachandran Plot Statistics				
no. of residues[c]	243	243	243	243
most favorable region (%)	93.8	93.8	92.9	93.8
allowed region (%)	5.2	5.7	6.7	5.7
generously allowed region (%)	1.0	0.5	0.5	0.5
disallowed (%)	0.0	0.0	0.0	0.0
Asymmetric Unit Content				
nonhydrogen protein atoms	2124	1999	2039	1984
biliverdin	43	43	43	43
water	287	254	298	284
PDB ID	3nb8	3nb9	3f0l	3f0m

[a] $R_{merge} = [\sum_h \sum_i |I_h - I_{hi}| / \sum_h \sum_i I_{hi}]$ where I_h is the mean of I_{hi} observations of reflection h. Numbers in parentheses represent highest resolution shell. [b] R-factor and R-free $= \sum ||F_{obs}| - |F_{calc}|| / \sum |F_{obs}| \times 100$ for 95% of recorded data (R-factor) or 5% of data (R-free). Numbers in parenthesis represent highest resolution shell. [c] Number of non-proline and non-glycine residues used for calculation.

the H3 helix between strands S4 and S5 in wild-type *PcyA* (*19*), which adopts a type I β-turn in both mutants, the D105N and H88Q structures have identical topology and superimpose with wild-type PcyA with an rmsd of 0.176 Å (243 equivalent Cα) and 0.223 Å (242 equivalent Cα) respectively.

The active sites of both mutants exhibit well-defined electron densities for the bound BV substrate, neighboring residues, and water molecules (Figure 2B,C). The most noticeable difference in both mutants compared to wild-type PcyA is the presence of an additional tightly bound water molecule (Wat400 in Figure 2B,C) located above the BV ring system (as viewed in Figure 2). The electron density assigned to this water (i.e., Wat400) is comparable with those of neighboring water molecules, ruling out its assignment to a bound metal ion. Wat400 also lies within hydrogen bonding distance to all four pyrrole nitrogen atoms of the BV substrate as well as to Oδ1 of Asn219 and Oγ1 of Thr222 (Figure 3). We also rule out assignment of this new electron density to an ammonium ion (present in the crystallization mixture) because the biochemical behavior in solution in the absence of ammonium sulfate is qualitatively identical to that in the crystal (*16*, *18*, *22*).

By comparison with wild-type PcyA, the overall active sites of both mutants appear to change little to accommodate this new water molecule. The BV substrate does translate ~0.25 Å out of the active site pocket for both mutants, however, although it essentially lies in the same plane as the wild-type substrate. In D105N, Oδ1 of Asn219 and Oγ1 of Thr222 move out by 0.22 Å and 0.45 Å, respectively, to ligate Wat400, with similar distances observed in H88Q. Such small structural perturbations suggest that the wild-type active site could also accommodate this water molecule, but this water is not seen in the wild-type PcyA structure (*19*).

Both mutant structures support the interpretation that the BV A-ring adopts the lactim tautomer (Figure 3). In this regard, the 2.81 Å distance between the BV O1 oxygen atom and Nδ1 of

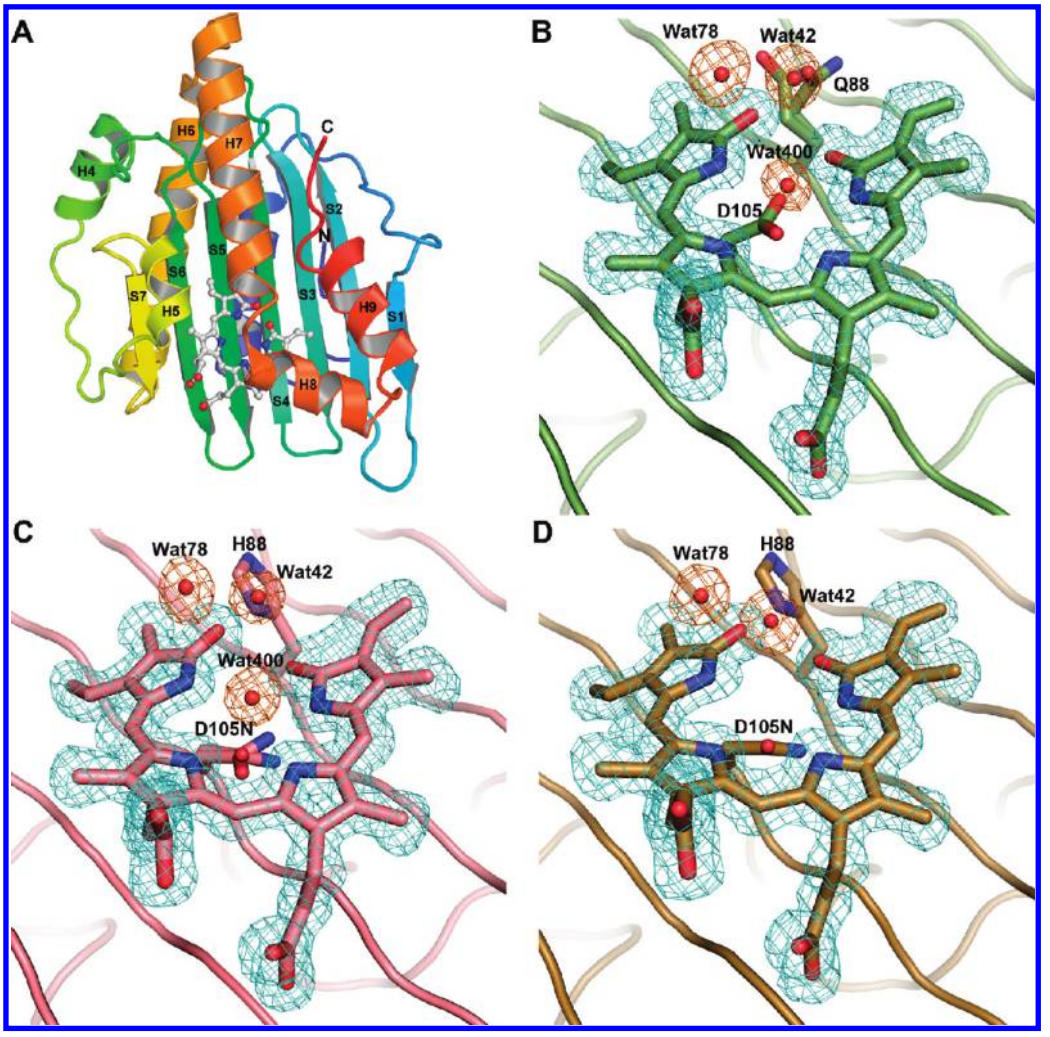

FIGURE 2: Structural models for BV-bound D105N and H88Q mutants of *Synechocystis* PcyA. (A) Overall structures of both mutants in their "oxidized" states are indistinguishable from those of wild-type PcyA. The protein backbone is depicted as a rainbow-shaded ribbon cartoon colored blue at the N-terminus and red at the C-terminus. Bound BV is shown in a ball-and-stick representation with white-colored carbon atoms. Cyan-colored electron density drawn at 1.0σ level for BV in the active site of "oxidized" (B) H88Q and (C) D105N mutants. Orange-colored electron density is contoured at 3σ from an annealed omit map (only waters omitted) revealing three tightly bound water molecules, one of which (i.e., Wat400) is missing in wild-type PcyA (*19*). (D) Wat400 is lost upon reduction of D105N (as shown) and H88Q (not shown) mutants.

His88 in the D105N mutant is an ideal H-bonding distance, implicating a strong hydrogen bond that requires the A-ring to assume the lactim tautomer (NMR data reveals that Nδ1 of His88 is deprotonated in D105N, see below). We have modeled the substrate in the bis-lactim tautomer to be consistent with previous EPR studies showing that upon reduction, the D105N BV radical resides in the bis-lactim state with both A- and D-ring oxygens being protonated (*22*). The assigned bis-lactim structure for bound substrate in H88Q is also fully consistent with the X-ray data.

Mutation of Asp105 and His88 Alters the Conformation of Key Catalytic Residues. Previous structural studies on BV-loaded wild-type PcyA have revealed dual conformations for Asp105 and Glu76, two conserved active-site residues that contact the BV substrate (*19*). Centered directly beneath BV, Asp105 adopts a major conformation (65% occupancy) that comprises a bidentate interaction with BV's D-ring. As depicted in Figure 1B, this "bidentate" conformer can adopt two tautomeric states corresponding to lactam and lactim isomers of the BV D-ring. In the minor "axial" conformation, the side chain of Asp105 carboxylic acid rotates ~90° relative to the major conformation with one δ-oxygen atom pointing toward the center of the bilin substrate. The δ-oxygen atom remains within H-bonding distance of all four pyrrole nitrogen atoms in this conformation. We assign this "axial" conformation to the ion-pair species in which Asp105's carboxylic acid proton is transferred to the bilin substrate (Figure 1B).

Comparative analysis of D105N and H88Q mutant structures with that of wild type reveals notable differences in interactions between the side chain of D105/N105 and the bound bilin substrate (Figure 3). For D105N, we observe dual conformations for the Asn105 side chain, however, these are rotated ~35° relative to each other. Both conformations are capable of only a single H-bonding contact with the D-ring pyrrole, e.g., Nδ2 of Asn105 H-bonding to the D-ring carbonyl or Oδ1 H-bonding to the D-ring nitrogen as depicted in Figure 3B. Not shown are other plausible Asn105 conformers in which the side chain amide nitrogen is pointing toward the center of the BV ring system (instead of oxygen); we disfavor this assignment because a clear H-bond is present between the main chain carbonyl of Leu87 and the side chain amide nitrogen of Asn105. At 1.3 Å resolution, however, we cannot assign the locations of hydrogen atoms on the bilin substrate so not all possible tautomers are depicted. As discussed later, NMR data indicate that His88 adopts the ε protonated tautomer as shown in Figure 3.

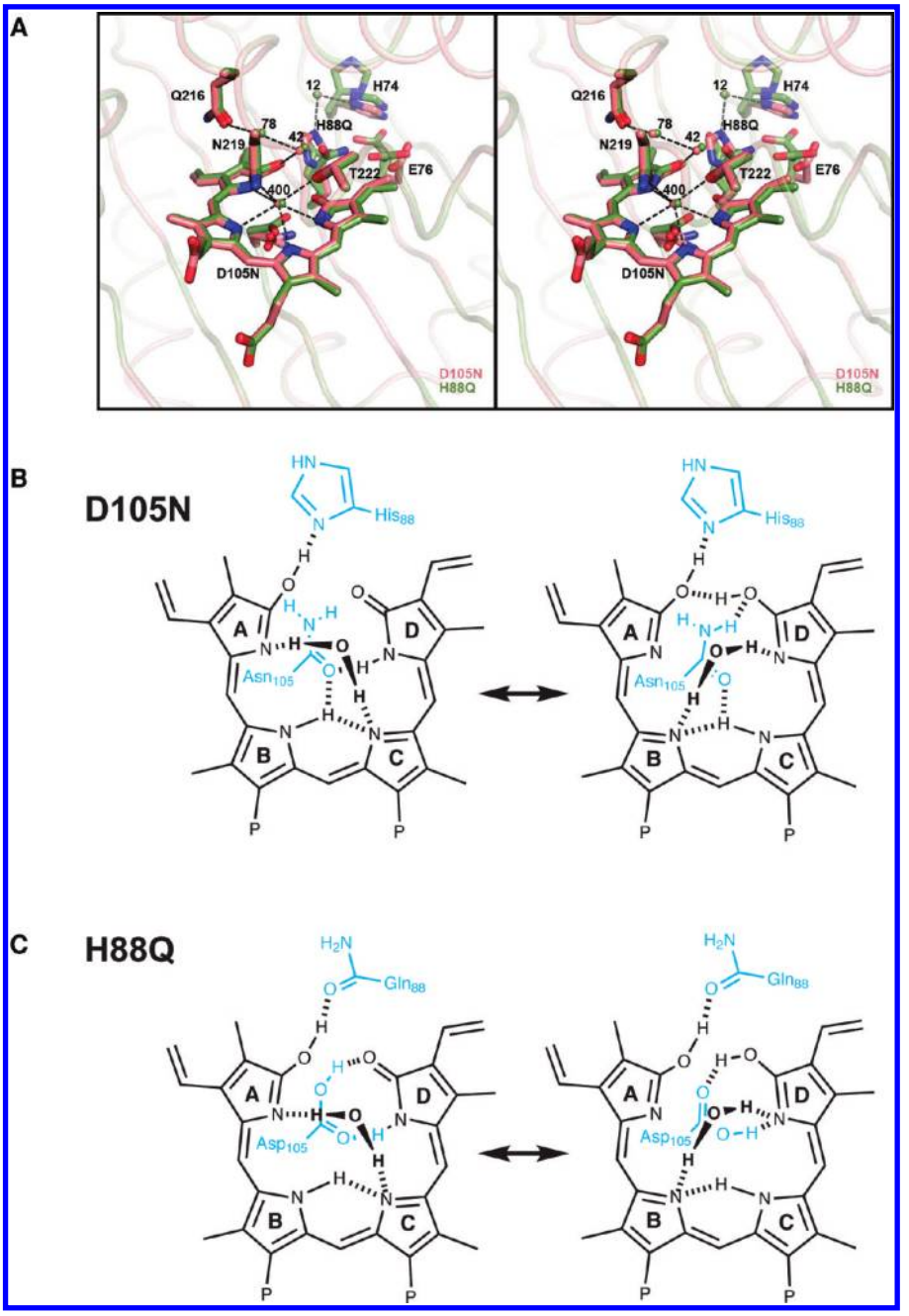

FIGURE 3: Active sites of PcyA D105N and H88Q mutants. (A) D105N (salmon) and H88Q (green) mutants superimpose with an rmsd of 0.172 Å for 242 equivalent α-carbons. BV substrate, conserved water molecules, and side chains of key residues are modeled in the active site. Many residues display multiple conformations (see text). Dashed lines denote potential hydrogen bonds in the D105N structure (3.5 Å H-bond distance cutoff) and ordered solvent molecules are colored in the same color as the carbons. (B) Monodentate lactim and lactam complexes of the BV D-ring bound to the D105N mutant. (C) Bidentate lactim and lactam complexes of the BV D-ring bound to the H88Q mutant. Protein residues are drawn in blue.

For the H88Q mutant, Asp105 adopts only one conformation that is very similar to the major bidentate conformation observed for wild type (Figure 3C). The distance between Oδ2 of Asp105 and the D-ring carbonyl oxygen (O19) is 2.5 Å for both H88Q and the major tautomer of wild type. This short distance implicates the presence of hydrogen atoms between both Asp105 oxygen atoms and the D-ring pyrrole system, consistent with the "neutral" Asp105 carboxylic acid-pyrrole chelate as depicted in Figure 3. Unlike wild-type PcyA however, an axial "ion-pair" conformer of D105/N105 (see Figure 1B) is not observed for either D105N or H88Q mutant.

It was previously shown that the carboxylic acid side chain of Glu76 lies extremely close to the D-ring vinyl group in wild-type PcyA (*19*). On the basis of this result and the evidence that mutation of Glu76 inhibits D-ring vinyl reduction but still catalyzes A-ring vinyl reduction (*18*, *21*), the hypothesis that Glu76 functions as the proton donor for D-ring vinyl reduction is well supported (*18*). It is thus notable that the side chain of Glu76 in the D105N mutant is located at a much larger distance from the BV substrate. In D105N, the closest contact between Oε2 of Glu76 and the 18^2 carbon of BV proved to be 2.96 Å while a Glu76 to BV-vinyl distance of 2.51−2.56 Å was measured for the wild type (*19*). Glu76 was located even more distant from the BV substrate in the H88Q mutant. Moreover, two conformations were observed in H88Q, one of these places the Glu76 side chain ~3.6 Å from the vinyl group while the other places Glu76 more

distant from the vinyl group adopting an apparent ion-pair interaction with His74 (see below). Taken together, these data show that the proton-donating Glu76 carboxylic acid side chain is poorly located for D-ring exovinyl group reduction in both D105N and H88Q mutants.

In addition to Asp105 and Glu76, other residues near the active site of the H88Q mutant display multiple conformations. Despite the single conformation for Asp105 in the H88Q mutant, the side chains of His74, Glu76, Gln88, and Tyr238 all adopt two conformations. In view of unreasonably close contacts for alternate conformations, we conclude that these dual conformations reflect two distinct global protein conformations rather than a heterogeneous combinatorial mixture. This suggests that coordinated movement of these residues plays a role in proton relay during catalysis as was previously proposed (*18*). In this regard, one of the two conformations of Gln88 corresponds to an H-bonding interaction with buried water molecule Wat12, which places Gln88's side chain too distant to interact with BV (Figure 3A). The other conformation of Gln88 is located within H-bonding distance to the O1 carbonyl oxygen of the BV A-ring. Because the exact conformation of Gln88's amide side chain cannot be unambiguously assigned from electron density maps at >1 Å resolution, two distinct structural models remain plausible for the orientation of the Gln88 side chain. We modeled an interaction such that the Oε1 oxygen atom is H-bonded to the A-ring lactim hydrogen with the Nε2 nitrogen atom interacting with Glu76 (Figure 3C). The A-ring lactim tautomer is consistent with the wild-type and D105N structures as well as EPR data on the semireduced radicals (*19*). However, a structural model with the amide group flipped, such that Nε2 interacts with the A-ring lactam O1 oxygen atom, remains plausible.

The Mutant-Specific, BV-Associated Water Is Lost upon One-Electron Reduction. Because the normal in vivo PcyA reductant ferredoxin (Fd) is too large to enter the crystal lattice to generate the one-electron reduced radical for structure determination of both D105N and H88Q mutants, we used sodium dithionite as an alternative chemical reducing agent (*34*, *35*). Dithionite-soaked crystals of both mutants led to a rapid color change from blue to green that was complete within 10 min (Supporting Information Figure 1). Dithionite-soaked crystals of both mutants also exhibited a characteristic *g* tensor ~2 EPR signal similar to ferredoxin-reduced mutants in solution (ref *22* and Supporting Information Figure 2), confirming the formation of a bilin radical.

In view of the potential for synchrotron-induced reduction reactions (*24*−*26*), a microspectrophotometer was used to monitor the UV/vis spectrum of dithionite-soaked crystals during the course of X-ray exposure. Indeed, prolonged exposure of a D105N crystal to X-rays led to decreased absorbance at ~660 and ~770 nm and increased absorbance at ~470 and ~720 nm (Supporting Information Figure 3A), a result that correlated well with the observed color change specifically within the region where the path of the X-ray beam passed through the crystal (Supporting Information Figure 3B). In view of this sensitivity to X-ray reduction, data collected from multiple dithionite-soaked crystals (aligned by crystal morphology) were merged, with each crystal receiving less than 1 min X-ray exposure corresponding to a radiation dose of 0.064 MGy. Data from 10 crystals of the reduced D105N mutant were merged to afford an R_{mrg} of 7.8% with 95% completeness at a resolution of 1.5 Å, while five merged crystals of the reduced H88Q mutant afforded data with an R_{mrg} of 7.9% with 81% completeness and a resolution of 1.5 Å (Table 1).

The most noticeable feature in the radical state structures of both mutants is the loss of the water molecule (Wat400) situated above its BV substrate (Figures 2D and 4). By contrast, all other bound water molecules near the active site, including the fully conserved water buried between His88 and His74, retain their locations and well-defined electron densities upon reduction. Asn219 and Thr222, whose side chains participate in H-bonds with Wat400, both move slightly closer to the BV substrate upon the release of Wat400 (Figure 4). Asn/Asp105 side chains are also pulled closer to the BV substrate upon reduction. These changes are consistent with the hypothesis that Wat400 provides a stabilizing H-bond and/or proton to the nascent BV radical and then exits the active site upon one electron reduction (see below).

In addition to the ejection of Wat400, movement of Wat42, centered above and between the A- and D-rings, accompanies BV reduction in D105N and H88Q mutants (Figure 4). Also conserved in wild type, Wat42 translates 0.83 and 0.93 Å upon reduction of the D105N and H88Q mutants, respectively. Such movement facilitates formation of a new H-bond with the A-ring pyrrole nitrogen by placing Wat42 0.7 Å closer to the A-ring pyrrole nitrogen which now lies within a distance of 3.1 Å. Wat42 also moves within H-bonding distance of the A-ring pyrrole oxygen O1, the side chain of Thr222, and another conserved water (Wat78) above the A-ring (Figure 4). It is reasonable that the formation of a new H-bond between Wat42 and the A-ring pyrrole nitrogen might function to shield the unpaired charge density on the BV substrate from the hydrophobic pocket of PcyA.

A number of other structural changes accompany reduction of both mutants. Residues that exhibit dual conformations in the oxidized state of H88Q (i.e., His74, Glu76, Tyr238) all adopt single conformations upon reduction that more closely resemble those of wild-type PcyA (Figures 4A,B). Interestingly, Asp105 retains a single bidentate conformation with paired H-bonds with the D-ring upon reduction (Figure 4B). Other more minor changes include a ~0.3 Å pivot of both B- and C-rings toward Asn219 and Thr222, and a greater separation between the A- and D-rings, which increase by ~0.2 and ~0.1 Å for D105N and H88Q mutants, respectively. The A-ring vinyl carbon 3^2 also tilts more out-of-plane upon reduction. For D105N, the D-ring vinyl group carbon 18^2, which lies noticeably out of plane in the oxidized state, moves more in plane with the conjugated D-ring pyrrole upon reduction. A similar change occurs in the D-ring vinyl group of H88Q, although this lies closer to planarity in the oxidized state.

Comparative NMR Analyses Reveal the Protonation States of Catalytically Important Histidine Residues in Wild-Type and Mutant PcyA. Because X-ray crystallography data at this resolution cannot resolve the location of dissociable hydrogen atoms, we employed NMR to probe the protonation state of histidine residues in wild-type and mutant ^{15}N-labeled PcyA preparations. The primary focus of these studies was the assignment of His88, which plays a key role in catalysis (*17*). Because ^{15}N NMR chemical shifts are diagnostic of histidine imidazole side chain protonation state, we particularly sought to determine whether His88's side chain is fully protonated or whether it adopts one of two neutral tautomers using this technique (*36*, *37*). PcyA contains six histidines, all of which are resolved as six sets of cross-peaks in two-dimensional

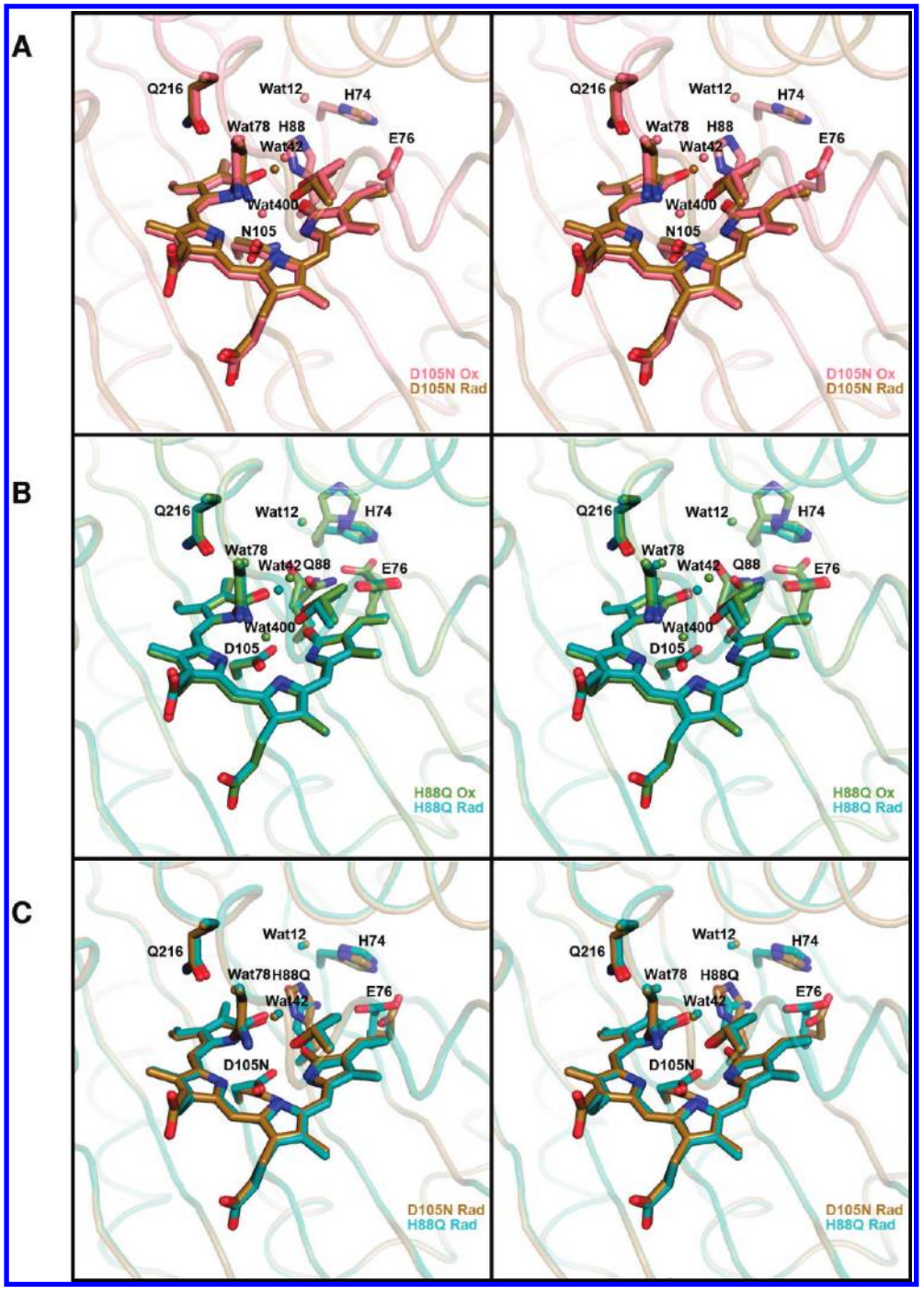

FIGURE 4: Structural comparison of semireduced bilin radical complexes of PcyA D105N and H88Q mutants with their oxidized states and with each other. (A) D105N oxidized (salmon color) and radical (sand color) structures. (B) H88Q oxidized (green) to H88Q radical (cyan) structures. (C) H88Q and D105N radical structures (coloring same as above). Water 400 departs in both radical structures.

$^{15}N-^{1}H$ LR-HMQC spectra of ^{15}N−labeled wild-type PcyA (Figure 5A and Supporting Information Table 1). Each cross-peak represents a 2-bond correlation of ^{1}H and ^{15}N resonances for the histidine imidazole ring, with Supporting Information Table 1 providing a list of chemical shifts for $^{1}H_{\delta 2}$, $^{1}H_{\varepsilon 1}$, $^{15}N_{\delta 1}$, and $^{15}N_{\varepsilon 2}$ resonances from each His residue for both substrate-free and BV-bound wild-type PcyA at pH 7.0.

Two-dimensional $^{15}N-^{1}H$ LR-HMQC spectra of wild-type PcyA, D105N, and H88Q mutant preparations all lacking bound BV substrate are compared in Figure 5A and in Supporting Information Figure 4. The His residue with the most downfield $^{1}H_{\varepsilon 1}$ chemical shift (8.55 ppm) and most upfield $^{1}H_{\delta 2}$ chemical shift (6.26 ppm) can be assigned to His88 because these resonances disappear in the spectrum of the H88Q mutant (green vs black peaks in Figure 5A). The chemical shifts of $^{15}N_{\delta 1}$ and $^{15}N_{\varepsilon 2}$ for His88 (assigned to 178 and 183 ppm, respectively) indicate that the imidazole side chain of His88 is fully protonated at pH 7.0 in BV-free wild-type PcyA. Interestingly, the His88 side chain chemical shifts remain unchanged when the pH was raised from 7.0 to 9.0, indicating the pK_a of His88 exceeds 9 for wild-type, BV-free PcyA (data not shown). This unusually high pK_a for His88 is consistent with the formation of an imidazolium-carboxylate ion-pair with Asp105, as was previously inferred from crystallography (*18*, *19*). NMR analysis of the D105N mutant reveals that this ion-pair interaction is disrupted as expected (Figure 5A, red). In this regard, the chemical shifts of the His88 NMR cross-peaks of the

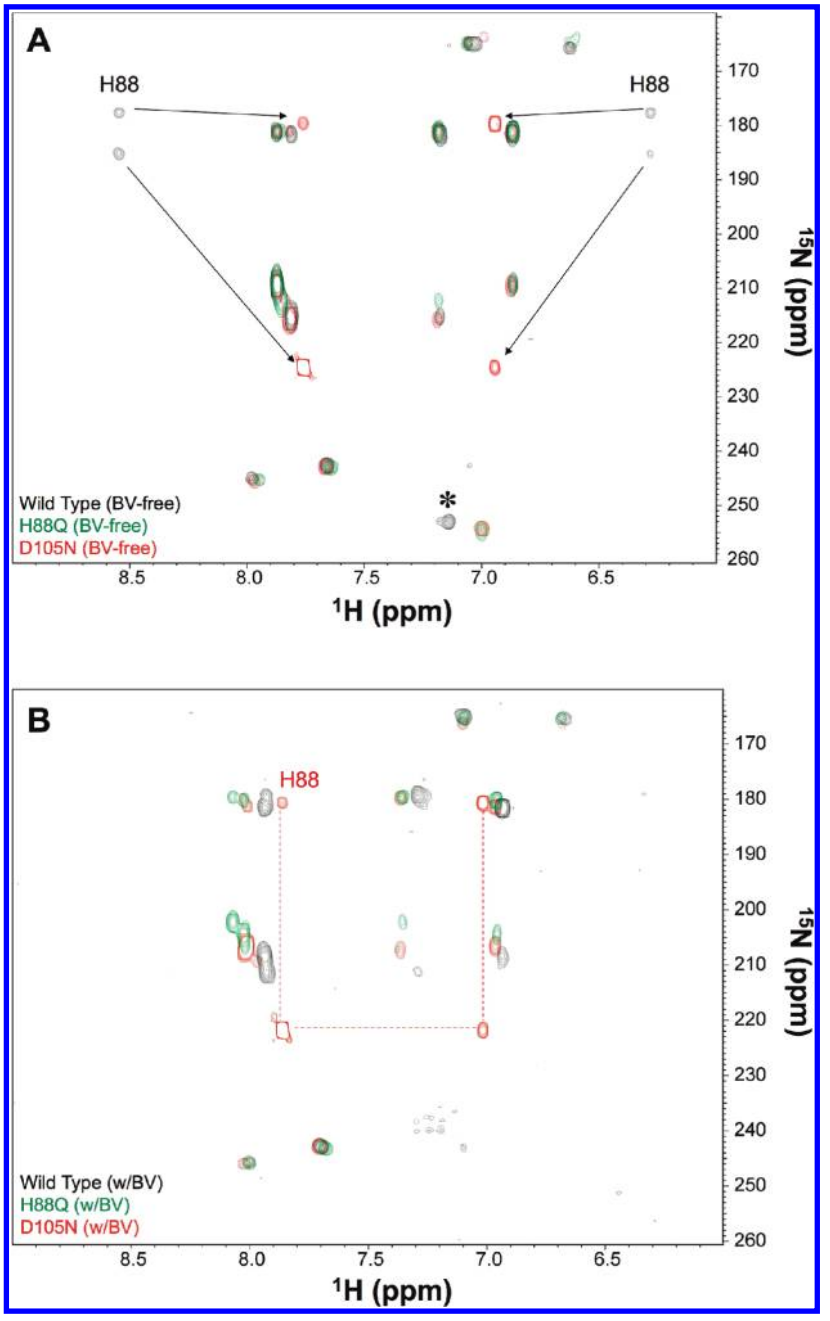

FIGURE 5: 2D ^{15}N−^{1}H LR-HMQC spectra of BV-free (A) and BV-bound (B) PcyA at pH 7.0. Spectra of wild type (black), H88Q (green) ,and D105N (red) are overlaid. Peaks at 8.55 and 6.30 ppm in (A) are assigned to His88. The peak at 7.12 ppm (marked by an asterisk) is assigned to His74 (data not shown). Dashed lines in red connect the set of resonances assigned to H88 in the BV-bound D105N mutant. Complete chemical shift assignments are given in Supporting Information Table 1 (see text for discussion).

BV-free D105N mutant are significantly different from those of wild-type PcyA (Figure 5A, black vs red peaks). The chemical shifts of $^{15}N_{\delta 1}$ and $^{15}N_{\varepsilon 2}$ for His88 in D105N are respectively 180 and 225 ppm, which indicates that His88 contains a neutral (Nε2 protonated tautomer) imidazole side chain in D105N at pH 7.0. On the basis of ^{15}N chemical shifts, it is clear that all other His residues in BV-free PcyA at pH 7.0 possess neutral imidazole side chains with protonated ε nitrogens and unprotonated δ nitrogens (Supporting Information Figure 4 and Supporting Information Table 1).

Two-dimensional ^{15}N−^{1}H LR-HMQC spectra of the three BV-bound PcyA species are compared in Figure 5B. Resolved cross-peaks from only four His residues are evident in the spectrum of BV-bound wild-type PcyA. This contrasts with substrate-free PcyA, whose six His residues are all resolved. On the basis of ^{15}N chemical shift assignments (Supporting Information Table 1), we conclude that all four His residues possess neutral imidazole side chains with protonated ε nitrogens and unprotonated δ nitrogens at pH 7.0 (as was observed in substrate-free wild-type PcyA). BV substrate binding in the PcyA active site correlates with the disappearance of cross-peaks at 6.26 and 8.55 ppm that are assigned to His88 in BV-free PcyA. Unexpectedly, none of the observed peaks in the BV-loaded wild-type spectrum are absent from the spectrum of the BV-loaded H88Q mutant (Figure 5B, green vs black peaks). Additionally, signals assigned to His74 are also missing in the spectrum of BV-loaded wild-type PcyA. While we attribute the absence of His88 and H74 signals in BV-loaded wild-type PcyA to exchange-broadening beyond detection, it is possible that signals for His88 and H74 are buried underneath those of other

histidines. Because protons can be shuttled between BV substrate and His88, between the two residues themselves that are interconnected by a H-bonded water molecule (Wat12), and also with bulk solvent via proton shuttle involving His74 (*18*), exchange broadening of His88 and His74 is not unexpected.

By contrast with the wild type, imidazole resonances at 7.05/220, 7.05/180, 7.90/220, and 7.90/180 ppm assigned to His88 for substrate-free D105N are retained upon BV binding (Figure 5A, B, connected by red dashes). Such cross-peaks, not observed in BV-bound wild type, indicate that His88 side chain adopts a neutral (Nε2 protonated) side chain in BV-loaded D105N. This observation is consistent with the hypothesis that insertion of the neutral Asn residue near His88 in the D105N mutant restores a more "typical" pK_a to His88, which adopts a neutral imidazole tautomer at pH 7.0. This line of reasoning also accounts for the dramatic sharpening of D105N's His88 signals and is consistent with the absence of these signals in the H88Q mutant (Figure 5B).

DISCUSSION

Mechanistic Implications of Structural Studies. The high-resolution crystal structures of both PcyA mutants in their oxidized and one-electron reduced radical states reported here provide new insight into the structural basis of the novel stability of the initial bilin radical intermediate. One of the most noticeable features of the X-ray structures centers around the dynamics of a novel water molecule (Wat400) associated with the BV substrate. This water molecule, not present in the crystal structure of wild type, is tethered to Asn219 and Thr222 side chains in addition to BV (Figure 3). Both radical structures reveal that this water molecule is ejected upon one-electron reduction. On the basis of this evidence, we propose that Wat400 donates a proton to the BV substrate upon the initial electron transfer to BV-loaded D105N, a process that leads to release of hydroxide ion as depicted in Figure 6. We envisage that $1e^-$ transfer to BV-loaded H88Q is accompanied by proton transfer from Asp105's carboxylic acid side chain and release of Wat400 (Figure 6C). Because the resulting bis-lactim radicals both lack the secondary proton donor, i.e., Glu76 that is in close contact with the bilin substrate in wild type (Figure 6A), further reduction of the semireduced D105N and H88Q radicals is unfavorable.

Recent crystal structures of the E76Q mutant of PcyA and of wild-type PcyA loaded with the stable intermediate DHBV indicate that both proteins also contain water molecules at a similar position to Wat400 (*21*). Like wild-type PcyA, however, two conformations of Asp105 were detected in both structures, a result consistent with partial protonation of the BV substrate and supported by the long wavelength absorption shoulder observed in the UV−visible spectrum of all three proteins (*18*, *21*). By contrast, neither an axial conformation for Asp105 nor the long wavelength shoulder were observed for either D105N and H88Q mutant. Because the E76Q mutant and wild-type both support A-ring reduction, we conclude that the axial bound water is required for reduction of the bilin A-ring.

In wild-type PcyA, it is well established that D-ring reduction precedes A-ring reduction (*15*) and the close association of the carboxylic side chain of Glu76 with the D-ring vinyl group well accounts for this result (*21*). By contrast, Glu76 is poorly located in both D105N and H88Q mutants to support D-ring vinyl reduction. We therefore propose that the premature binding and release of the axial water (i.e., Wat400) also accounts for the inability of D105N and H88Q mutants to support A-ring reduction. The radical intermediates of the D105N and H88Q mutants are thus unable to accept an additional electron for either D- or A-ring vinyl reduction and remain catalytically stalled in their radical states, as they lack suitable proton donors in direct contact with the substrate.

Mechanistic Implications of ^{15}N NMR Studies. Previous crystallographic analyses reveal two conformations of Asp105 in the substrate-bound wild-type PcyA (*19*). We interpret these dual conformational states to correspond to a mixture of a neutral, unprotonated BV species (major) and a cationic, O-protonated BV species (minor). These two states are shown in Figure 1B, with the major conformation assigned to a neutral, "bidentate" H-bonding interaction of Asp105 with the D-ring pyrrole, while the minor "axial" conformation assigned to a BVH^+:$Asp105^-$ ion pair. For the latter, the resulting positive charge not only can be delocalized within BV's π-system but also can be further stabilized by transfer to the imidazole groups of His88 and His74. This extensive proton delocalization network likely accounts for the loss of NMR signals for both His88 and His74 imidazole side chains upon BV binding due to exchange broadening resulting from interconversion between the many possible tautomeric species. By contrast, we observe resolved NMR signals for the His88 and His74 imidazole side chains of the D105N mutant (and for His74 of the H88Q mutant), indicating that exchange broadening is not present in these complexes as might be expected because there are many fewer tautomeric forms for the D105N mutant (Supporting Information Figure 5B).

While the normal course of BV reduction by PcyA occurs via sequential reduction of its exo- and endovinyl groups, PcyA can metabolize the biliverdin XIIIα (BV13) isomer, which lacks a D-ring exovinyl group, to generate the A-ring reduced iso-PΦB (*15*, *17*). The PcyA H88Q and D105N mutants are also impaired in BV13 turnover and can only catalyze the first electron reduction of BV13, also trapping BV13 in a one-electron-reduced radical state (*16*). Considering that the wild-type enzyme does not release its two electron reduced 18^1,18^2-DHBV intermediate, this result argues that His88 must be reprotonated for full vinyl group reduction. We previously proposed a potential proton relay system that may be able to reprotonate His88 (*18*). In this regard, the Nε2 nitrogen of His88 forms a H-bond to a water molecule buried in the protein core (Wat12), which in turn hydrogen bonds to His74. His74 resides close to Lys72, which in turn resides next to Arg71. The latter two conserved residues make an unusual β-bulge, bringing both side chains next to each other in the β-strand. This buried water molecule (Wat12) appears important for activity, because changing His74, which hydrogen bonds to the water, to other hydrogen-bonding residues like Asn, Gln, Asp, or Glu only reduces activity slightly, while the H74A mutant dramatically diminished activity to less that 1% (*17*). On the basis of this line of reasoning, all mutations that disrupt this proton relay such as H88Q and D105N should be catalytically stalled, a prediction that can be tested by additional site-directed mutagenesis.

A Revised Catalytic Mechanism for Wild-Type PcyA. On the basis of the X-ray structural and NMR spectroscopic data, we propose a revised mechanism for the sequential reduction of BV to PCB by wild-type PcyA. As shown in Figure 7, we envisage that the initial $2e^-$ reduction of BV to DHBV proceeds essentially as that proposed previously (*18*). Although the initial major species of the bound substrate is neutral, it is likely that the minor protonated species accepts the initial electron to yield a neutral radical intermediate. This radical intermediate can adopt many interconverting neutral and zwitterionic tautomers, only

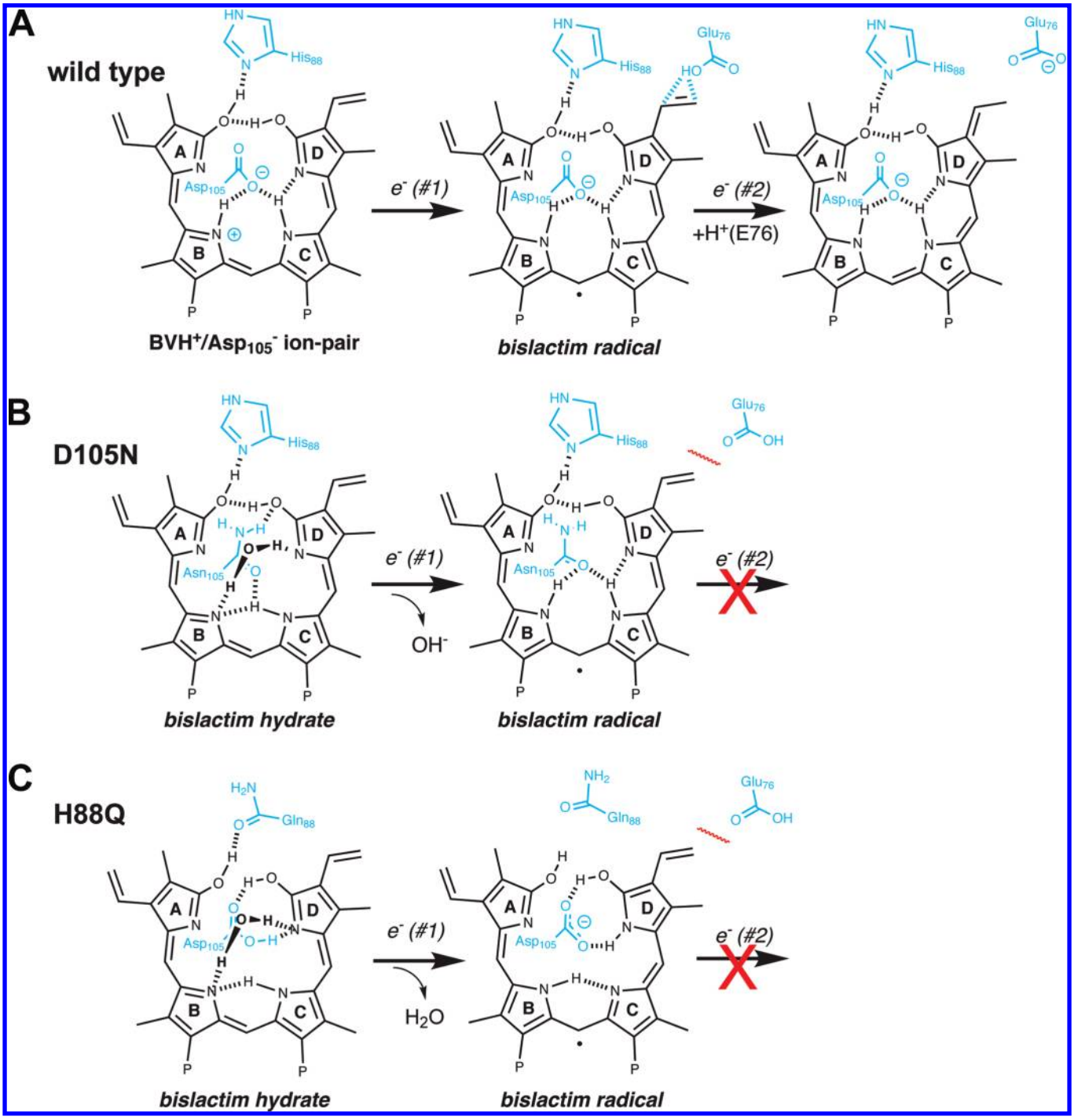

FIGURE 6: Proposed structural models for one electron reduction of wild-type, D105N, and H88Q PcyA. (A) The BVH^+/Asp^- ion pair accepts the initial electron in wild-type PcyA to generate a neutral radical intermediate. Glu76 is ideally positioned for the second proton-couple electron transfer. For both D105N (B) and H88Q (C) mutants, BV is not protonated and Glu76 is poorly positioned for secondary electron transfer. For D105N, one electron transfer to enzyme-bound substrate is accompanied by proton transfer from Wat400 and ejection of hydroxide ion. For H88Q, proton-coupled electron transfer mediated by Asp105 instead results in ejection of water. Protein residues are drawn in blue.

one of which, i.e., the bis-lactim radical, is shown in Figure 7. The close apposition of Glu76 carboxylic acid side chain to the D-ring vinyl group provides a strong rationale for the preference of D-ring reduction upon the transfer of the second electron, a reaction that yields the stable DHBV intermediate. It is particularly interesting that, unlike the D105N and H88Q mutants, both of which are catalytically stalled, the E76Q mutant retains the ability to reduce the A-ring vinyl group to produce the unnatural $2e^-$ reduced product phytochromobilin (*18*, *21*). This argues that the lack of close association of the Glu76 carboxylic acid side chain seen in D105N and H88Q mutants is insufficient justification for their inability to accept two electrons.

For A-ring reduction by wild-type PcyA, we propose that an axial water plays a key role in the reduction of DHBV to PCB. In this regard, the recent crystal structure of DHBV-loaded PcyA reveals the presence of an axial water molecule in the identical position to Wat400 in BV-loaded D105N and H88Q mutants (*21*). We propose that hydration of the DHBV intermediate occurs prior to subsequent electron transfer. Important to the subsequent reduction, hydration would also help retain the DHBV

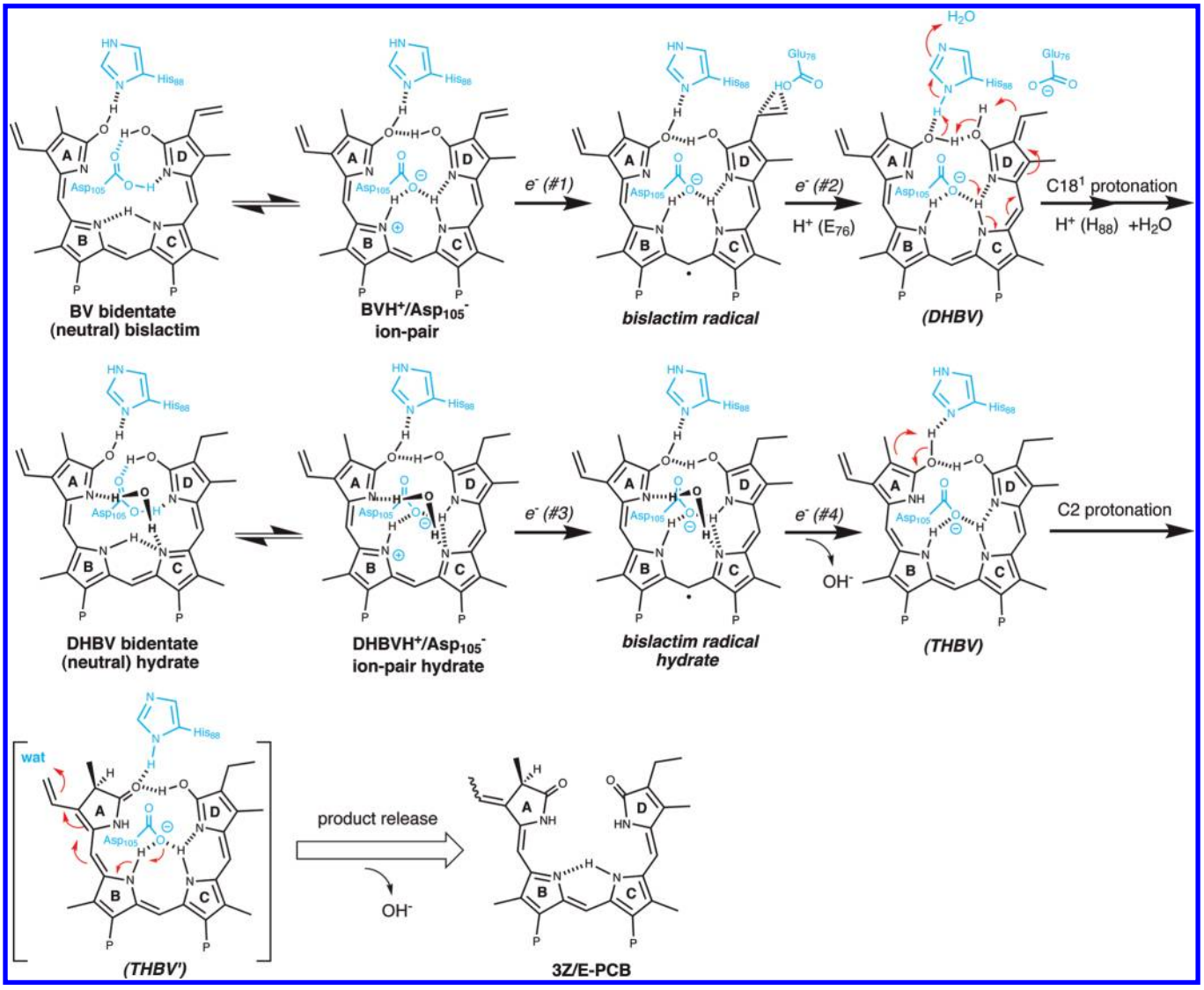

FIGURE 7: A revised catalytic mechanism for wild-type PcyA is based on structural data. See Discussion for details.

intermediate in the active site. Absorption measurements show that, like BV, DHBV is also partially protonated when bound to wild-type PcyA (*15*). We envisage that this hydrated, cationic DHBV species accepts the third electron to yield a neutral semireduced radical species. Unlike the D105N and H88Q mutants, we propose that the axial water is not ejected at this step because it provides the proton needed to yield the fully reduced tetrahydrobiliverdin (THBV) intermediate that ultimately rearranges to PCB as formalized in Figure 7. We therefore conclude that premature binding and expulsion of the axial water in the D105N and H88Q mutants accounts for the unusual stability of the semireduced bilin radical intermediate(s).

Because proton localization and the dynamics of proton transfer are critical to understanding the catalytic mechanism and regiospecificity of the various members of the FDBR family, ongoing research must leverage vibrational and magnetic resonance spectroscopies to fully resolve the assumptions underlying this proposed mechanism. In this regard, magnetic resonance has already proven useful for assessment of histidine protonation states in wild-type and mutant species of PcyA. In conjunction with recombinant forms of wild-type and mutant PcyA species containing stable isotope labeled amino acid and/or bilin analogues, such studies provide a powerful approach for fully understanding the structural basis of bilin reduction and regiospecificity of this interesting family of radical enzymes.

ACKNOWLEDGMENT

We thank Nathan C. Rockwell for critical reading of the manuscript. Portions of this research were carried out at the Stanford Synchrotron Radiation Lightsource, a national user facility operated by Stanford University on behalf of the U.S. Department of Energy, Office of Basic Energy Sciences. The SSRL Structural Molecular Biology Program is supported by the Department of Energy, Office of Biological and Environmental Research, and by the National Institutes of Health, National Center for Research Resources, Biomedical Technology Program, and the National Institute of General Medical Sciences.

SUPPORTING INFORMATION AVAILABLE

Picture of crystal of PcyA D105N at start of addition of 100 mM sodium dithionite, picture of same crystal 10 min after dithionite addition; 130 GHz pulsed EPR spectrum of radical intermediate of H88Q crystal at 45 K; microspectrometry of PcyA D105N mutant crystal in the X-ray beam at beamline 7-1 at SSRL, picture of crystal after a 6 min exposure to synchrotron

radiation; resonance assignments for $^{15}N-^{1}H$ LR-HMQC spectrum of BV-free PcyA at pH 7.0; NMR chemical shifts of histidine imidazole side chain resonance. This material is available free of charge via the Internet at http://pubs.acs.org.

REFERENCES

1. McDonagh, A. F. (1979) Bile Pigments: Bilatrienes and 5,15-Biladienes, in The Porphyrins (Dolphin, D., Ed.), pp 293−491, Academic Press, New York.
2. Ortiz de Montellano, P. R., Auclair, K. (2003) Heme Oxygenase Structure and Mechanism, in The Porphyrin Handbook. The Iron and Cobalt Pigments: Biosynthesis, Structure and Degradation (Guilard, R., Ed.), pp 183−210, Academic Press, New York City.
3. Beale, S. I. (2002) Biosynthesis of phycobilins. *Chem. Rev. 93*, 785–802.
4. Frankenberg, N., Lagarias, J. C. (2003) Biosynthesis and Biological Function of Bilins, in The Porphyrin Handbook. Chlorophylls and Bilins: Biosynthesis Structure and Degradation. (Guilard, R., Ed.), pp 211−235, Academic Press, New York.
5. Rockwell, N. C., Su, Y. S., and Lagarias, J. C. (2006) Phytochrome structure and signaling mechanisms. *Ann. Rev. Plant Biol. 57*, 837–858.
6. Glazer, A. N. (1988) Phycobiliproteins. *Methods Enzymol. 167*, 291–303.
7. Wilks, A. (2002) Heme oxygenase: evolution, structure, and mechanism. *Antioxid. Redox Signal. 4*, 603–614.
8. Mantle, T. J. (2002) Haem degradation in animals and plants. *Biochem. Soc. Trans. 30*, 630–633.
9. Maines, M. D. (2004) The heme oxygenase system: past, present, and future. *Antioxid. Redox Signal. 6*, 797–801.
10. Maines, M. D. (2005) New insights into biliverdin reductase functions: linking heme metabolism to cell signaling. *Physiology* (*Bethesda*) *20*, 382–389.
11. Maines, M. D., and Trakshel, G. M. (1993) Purification and characterization of human biliverdin reductase. *Arch. Biochem. Biophys. 300*, 320–326.
12. Frankenberg, N., Mukougawa, K., Kohchi, T., and Lagarias, J. C. (2001) Functional genomic analysis of the HY2 family of ferredoxin-dependent bilin reductases from oxygenic photosynthetic organisms. *Plant Cell 13*, 965–978.
13. Dammeyer, T., Hofmann, E., and Frankenberg-Dinkel, N. (2008) Phycoerythrobilin synthase (PebS) of a marine virus—crystal structures of the biliverdin complex and the substrate-free form. *J. Biol. Chem. 283*, 27547–27554.
14. Wedemayer, G. J., Wemmer, D. E., and Glazer, A. N. (1991) Phycobilins of cryptophycean algae. Structures of novel bilins with acryloyl substituents from phycoerythrin 566. *J. Biol. Chem. 266*, 4731–4741.
15. Frankenberg, N., and Lagarias, J. C. (2003) Phycocyanobilin:ferredoxin oxidoreductase. Biochemical and spectroscopic characterization. *J. Biol. Chem. 278*, 9219–9226.
16. Tu, S.-L., Gunn, A., Toney, M. D., Britt, R. D., and Lagarias, J. C. (2004) Biliverdin reduction by cyanobacterial phycocyanobilin:ferredoxin oxidoreductase (PcyA) proceeds via linear tetrapyrrole radical intermediates. *J. Am. Chem. Soc. 126*, 8682–8693.
17. Tu, S.-L., Sughrue, W., Britt, R. D., and Lagarias, J. C. (2006) A conserved histidine−aspartate pair is required for exovinyl reduction of biliverdin by a cyanobacterial phycocyanobilin:ferredoxin oxidoreductase. *J. Biol. Chem. 281*, 3127–3136.
18. Tu, S.-L., Rockwell, N. C., Lagarias, J. C., and Fisher, A. J. (2007) Insight into the Radical Mechanism of Phycocyanobilin-Ferredoxin Oxidoreductase (PcyA) Revealed by X-ray Crystallography and Biochemical Measurements. *Biochemistry 46*, 1484–1494.
19. Hagiwara, Y., Sugishima, M., Takahashi, Y., and Fukuyama, K. (2006) Crystal structure of phycocyanobilin:ferredoxin oxidoreductase in complex with biliverdin IXalpha, a key enzyme in the biosynthesis of phycocyanobilin. *Proc. Natl. Acad. Sci. U.S.A 103*, 27–32.
20. Hagiwara, Y., Sugishima, M., Takahashi, Y., and Fukuyama, K. (2006) Induced-fitting and electrostatic potential change of PcyA upon substrate binding demonstrated by the crystal structure of the substrate-free form. *FEBS Lett. 580*, 3823–3828.
21. Hagiwara, Y., Sugishima, M., Khawn, H., Kinoshita, H., Inomata, K., Shang, L., Lagarias, J. C., Takahashi, Y., and Fukuyama, K. (2010) Structural insights into vinyl reduction regiospecificity of phycocyanobilin:ferredoxin oxidoreductase (PcyA). *J. Biol. Chem. 285*, 1000–1007.
22. Stoll, S., Gunn, A., Brynda, M., Sughrue, W., Kohler, A. C., Ozarowski, A., Fisher, A. J., Lagarias, J. C., and Britt, R. D. (2009) Structure of the biliverdin radical intermediate in phycocyanobilin:ferredoxin oxidoreductase identified by high-field EPR and DFT. *J. Am. Chem. Soc. 131*, 1986–1995.
23. Matthews, B. W. (1968) Solvent content of protein crystals. *J. Mol. Biol. 33*, 491–497.
24. Chance, B., Angiolillo, P., Yang, E. K., and Powers, L. (1980) Identification and assay of synchrotron radiation-induced alterations on metalloenzymes and proteins. *FEBS Lett. 112*, 178–182.
25. Berglund, G. I., Carlsson, G. H., Smith, A. T., Szoke, H., Henriksen, A., and Hajdu, J. (2002) The catalytic pathway of horseradish peroxidase at high resolution. *Nature 417*, 463–468.
26. Wuerges, J., Lee, J. W., Yim, Y. I., Yim, H. S., Kang, S. O., and Carugo, K. D. (2004) Crystal structure of nickel-containing superoxide dismutase reveals another type of active site. *Proc. Natl. Acad. Sci. U.S.A. 101*, 8569–8574.
27. Paithankar, K. S., and Garman, E. F. (2010) Know your dose: RADDOSE. *Acta Crystallogr., Sect. D: Biol. Crystallogr. 66*, 381–388.
28. Emsley, P., and Cowtan, K. (2004) Coot: model-building tools for molecular graphics. *Acta Crystallogr., Sect. D: Biol. Crystallogr. 60*, 2126–2132.
29. Murshudov, G. N., Vagin, A. A., and Dodson, E. J. (1997) Refinement of macromolecular structures by the maximum-likelihood method. *Acta Crystallogr., Sect. D: Biol. Crystallogr. 53*, 240–255.
30. Laskowski, R. A., W.A, M., Moss, D. S., and Thornton, J. M. (1993) PROCHECK: a program to check the stereochemical quality of protein structures. *J. Appl. Crystallogr. 26*, 283–291.
31. Marley, J., Lu, M., and Bracken, C. (2001) A method for efficient isotopic labeling of recombinant proteins. *J. Biomol. NMR 20*, 71–75.
32. Pelton, J. G., Torchia, D. A., Meadow, N. D., and Roseman, S. (1993) Tautomeric states of the active-site histidines of phosphorylated and unphosphorylated IIIGlc, a signal-transducing protein from *Escherichia coli*, using two-dimensional heteronuclear NMR techniques. *Protein Sci. 2*, 543–558.
33. Shaka, A. J., Barker, P. B., and Freeman, R. (1985) Computer-Optimized Decoupling Scheme For Wideband Applications And Low-Level Operation. *J. Magn. Reson. 64*, 547–552.
34. Jellinek, K. (1911) Concerning the electrolytic potential of hydrosulphite reactions. *Z. Elektrochem. Angew. Phys. Chem. 17*, 157–176.
35. Mayhew, S. G. (1978) The redox potential of dithionite and SO_2 from equilibrium reactions with flavodoxins, methyl viologen and hydrogen plus hydrogenase. *Eur. J. Biochem. 85*, 535–547.
36. Drohat, A. C., Xiao, G., Tordova, M., Jagadeesh, J., Pankiewicz, K. W., Watanabe, K. A., Gilliland, G. L., and Stivers, J. T. (1999) Heteronuclear NMR and crystallographic studies of wild-type and H187Q *Escherichia coli* uracil DNA glycosylase: electrophilic catalysis of uracil expulsion by a neutral histidine 187. *Biochemistry 38*, 11876–11886.
37. Farr-Jones, S., Wong, W. Y. L., Gutheil, W. G., and Bachovchin, W. W. (1993) Direct observation of the tautomeric forms of histidine in nitrogen-15 NMR spectra at low temperatures. Comments on intramolecular hydrogen bonding and on tautomeric equilibrium constants. *J. Am. Chem. Soc. 115*, 6813–6819.